Indian Journal of Chemistry
Vol. 58A, June 2019, pp. 637-644

Photocatalytic activity of natural clay Bentonite supported $ZnWO_4$

G Ida[a,b], K Thirumalai[c], M Swaminathan*[,d] & D Easwaramoorthy*[,e]

[a]Research and Development Centre, Bharathiar University, Coimbatore 641 046, India

[b]Department of Chemistry, Dhaanish Ahmed College of Engineering, Chennai 601 301, India

[c]PG & Research Department of Chemistry, Govt. Arts College, Tiruvannamalai 606 603, India

[d]Nanomaterials Laboratory (IRC), Department of Chemistry, Kalasalingam University, Krishnankoil 626 126, India

[e]Department of Chemistry, B S Abdur Rahman University, Vandalur, Chennai 600 048, India

Email: Chemsam50@gmail.com (M S)/ easwar@bsauniv.ac.in (D E)

Received 5 June 2018; revised and accepted 29 April 2019

Natural clay Bentonite supported $ZnWO_4$ has been successfully synthesized through hydrothermal-thermal decomposition method. The experimental results reveal that 12 wt% of Bentonite supported $ZnWO_4$ exhibited higher photocatalytic activity for the degradation of two basic dyes (Rhodamine-B (Rh-B) and Methylene Blue (MB) under UV light than prepared $ZnWO_4$. Bentonite-$ZnWO_4$ (BZW) was characterized by X–ray powder diffraction (XRD), field emission scanning electron microscopy (FE–SEM), energy dispersive spectroscopy (EDS), field emission transmission electron microscopy (FE–TEM), X-ray photo electron spectroscopy (XPS), photoluminescence spectroscopy (PL), UV–Vis diffuse reflectance spectroscopy (DRS**)** and BET surface area analysis. FESEM images exhibit the formation of microflakes, which have been joined together by an edge-to-flat-surface conjunction. From the BET analysis it has been found that BZW has higher surface than prepared $ZnWO_4$. As synthesized Bentonite supported $ZnWO_4$ has high recyclability for four successive cycles.

Keywords: Bentonite clay, Zinc tungstate ($ZnWO_4$), Microflakes, Heterostructure, Basic dyes

Heterogeneous photocatalysis has been considered as an ecofriendly process in the past few decades[1-3]. Particularly, semiconductor photocatalytic degradation of organic pollutants has good potential for environmental purification[4-6]. In the semiconductor photocatalytic degradation process choice of metals and metal oxides is challenging for better catalytic activity. Mixed metal oxide nanomaterials have found remarkable importance due to their wide applications in different interdisciplinary fields[7-10]. The transition metal tungstates with formula MWO_4 attracted much attention due to their physico-chemical, structural, and photoluminescence characteristics[11,12]. Transition metal tungstates form an important class of functional materials as they possess a combination of covalent, ionic and metallic bonding. Their unique symmetry dependent and spontaneous polarization properties render them with important characteristics like ferroelectricity, conductivity and photoluminescency[13]. Transition metal tungstates, due to their unique chemical properties, are very useful for many potential applications such as supercapacitor and photocatalytic material[14-18], LED, magnetic and fluorescent materials[19-21], optical fiber, humidity sensors[22], light emitting materials[23, 24], scintillator[25] and laser host[26]. $ZnWO_4$ was investigated as a promising photocatalyst for water splitting and pollutant mineralization[27-29]. Clays find growing application in wastewater treatment as adsorbents due to their wide availability, low-cost and good intrinsic adsorption characteristics. A number of natural clays including kaolin, bentonite and zeolite are used for the removal of chemical pollutants from wastewater[30-32]. Natural clay Bentonite consists of montmorillonite with larger surface area, high cation exchange capacity and negative surface charge. These different properties help to absorb various metals and dyes on their surface which is useful for wastewater treatment[33, 34]. In the present work, we successfully prepared natural clay bentonite supported $ZnWO_4$ and investigated its catalytic efficiency by the mineralisation of Rhodamine-B and Methylene Blue dyes with UV irradiation.

Materials and Methods

Zinc nitrate hexahydrate ($Zn(NO_3)_2.6H_2O$), Sodium tungstate dihydrate ($Na_2WO_4.2H_2O$), Sodium

hydroxide and ethanol were received from Himedia chemicals. Rhodamine-B (Rh-B) and Methylene Blue (MB) dyes were supplied by Colour Chem, Pondicherry. (Rh-B, molecular formula: $C_{28}H_{31}ClN_2O_3$ and molecular weight: 479.02 $gmol^{-1}$; MB, molecular formula: $C_{16}H_{18}N_3SCl$; molecular weight: 319.86 $gmol^{-1}$). Bentonite was obtained from Sigma and used as received without pretreatment, with the exception of washing to eliminate soluble impurities. TiO_2-P25 was used to compare photocatalytic activity.

Preparation of Bentonite supported $ZnWO_4$ (BZW)

Under vigorous stirring, 1.649 g of $Na_2WO_4.2H_2O$ (0.05 M) solution was added to 0.4 M of $Zn(NO_3)_2.6H_2O$ (11.90 g). To this $ZnWO_4$, 0.275 g of Bentonite (12 wt%) dispersed in 10 mL ethanol was added at pH 10 adjusted with NaOH solution. This precipitate of Zinc tungstate with Bentonite was treated hydrothermally (115 °C for 12 h), and calcined (500 °C for 12h) to obtain Bentonite loaded $ZnWO_4$. Catalysts with 9 and 15 wt% Bentonite on $ZnWO_4$ were prepared by changing the amount of bentonite using the same method as mentioned above.

Catalyst characterization

Details of the instruments used for characterization by XRD, FE-SEM, EDS, FE-TEM, XPS, DRS and Photoluminescence are reported in our earlier papers[35,40-41]. X-Ray diffraction (XRD) patterns were recorded with a Siemens D5005 diffractometer using copper (Cu) Ka (k = 0.151 418 nm) radiation. Surface morphology was studied by using a field emission scanning electron microscope (FE-SEM) (Model Carl Zeiss Evo 18). X-Ray photoelectron spectra of the catalysts were recorded in an ESCA-3 Mark II spectrometer (VG Scientific Ltd, England, UK) using aluminium (Al) Ka (1486.6 eV) radiation as the source. Diffuse reflectance spectra were recorded with Shimadzu UV-2450. The photoluminescence (PL) spectra of the samples were recorded on a PerkinElmer LS 55 fluorescence spectrometer.

Photocatalytic activity

All experiments were carried out under identical conditions using Heber multilamp photoreactor model HML-MP 88. The detail of this model is described elsewhere[35]. The absorbance at 259 and 293 nm represents the aromatic content of Rh-B and MB respectively and their decrease indicates the degradation of dye.

Results and Discussion

XRD analysis of Bentonite-$ZnWO_4$

Crystallinity of the prepared photocatalyst Bentonite-$ZnWO_4$ is analyzed using XRD (Fig. 1). XRD patterns of the prepared $ZnWO_4$, raw Bentonite and Bentonite supported $ZnWO_4$ are shown in Fig. 1a and 1b respectively. The diffraction peaks of prepared $ZnWO_4$ at 27.62°, 31.65°, 33.99°, 36.36°, 42.46°, 47.53°, 56.55°, 63.28° and 67.66° corresponding to (111), (020), (021), (121), (211), (112), (212), (113) and (041) planes of monoclinic primitive $ZnWO_4$ are given in Fig. 1a, and these values matched with JCPDS card number 15-0774 [36]. The new peaks observed at peaks at 2θ = 19.8°, 26.2°, 27.6°, 50.5°, 57.7° and 79.5° in raw Bentonite (Fig. 1b) are assigned to the (100), (111), (002), (003), (121) and (114) planes of raw bentonite. This shows presence of montmorillonite, quartz and calcite in bentonite (JCPDS cards for observed phase are: montmorillonite (cristobalite) 13-0135, quartz 89-8936, calcite 83-0578)[37]. The average crystallite size of Bentonite-$ZnWO_4$, determined from Scherrer formula (equation 1) is 36.8 nm.

$$\Phi = \frac{K\lambda}{\beta \cos\theta}$$

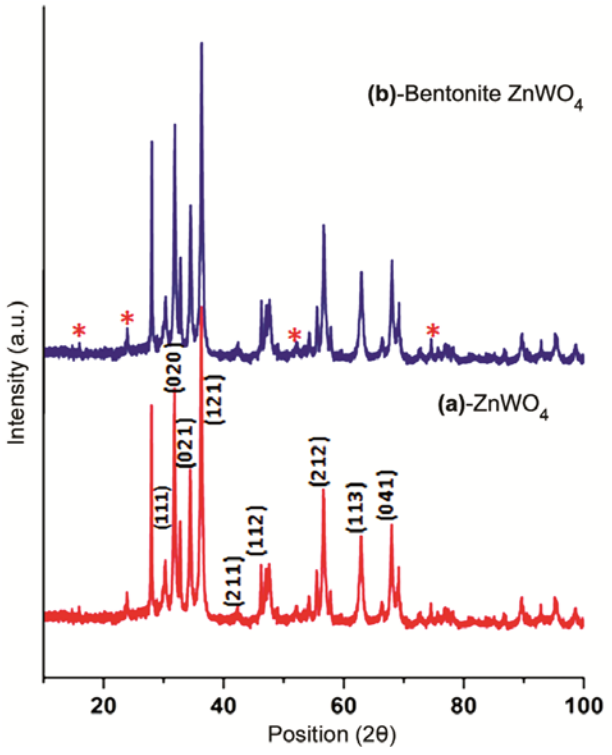

Fig. 1 — XRD patterns of (a) Prepared $ZnWO_4$, and, (b) Bentonite- $ZnWO_4$.

Surface morphology of Bentonite-$ZnWO_4$

The sizes, morphologies and microstructure of the as-prepared samples were exposed by FE-SEM and FE-TEM techniques. Low magnification SEM images of the Bentonite-$ZnWO_4$ (shown in Fig. 2a-d) indicate that prepared catalyst Bentonite-$ZnWO_4$ has flakes morphology with intermittent nanoparticles. The morphologies observed on the particle surface might be due to the impact of Bentonite particles. The microstructures are highly porous and most of the microflakes consist of large quantities loosely clustered together therefore such architecture is a result of some kind of self-assembly rather than random aggregation. Relatively the microscale hierarchical structures have large numbers of mesopores which can serve as transmission paths to enhance the transfer rate of organic molecules.

FE-TEM images of Bentonite-$ZnWO_4$ are shown in Fig. 3a-d. The uniform distribution of elements predicts the close attachment within oxides, where particles appear as spherical and hexagonal shapes. The dark portion in images shows the presence of Bentonite clay on the surface of $ZnWO_4$.

The survey spectrum of Bentonite-$ZnWO_4$ photocatalyst is given in Fig. 4a and it mainly consists of zinc, oxygen and tungsten along with weak carbon peak and peaks of other elements of Bentonite. The XPS spectra of Zn 2p are shown in Fig. 4b and the peak positions of Zn $2p_{1/2}$ and Zn $2p_{3/2}$ orbitals are located at 1045.81 and 1022.66 eV respectively. From these peaks, we can conclude that zinc is in the oxidation state of Zn^{2+} [38]. Binding energies at 35.66 and 37.77 eV are assigned for Tungsten W ($4f_{7/2}$) and W ($4f_{5/2}$) respectively (Fig. 4c). It is confirmed that tungsten ion is present in +6 oxidation state[39]. Binding energy peak of O 1s is asymmetric (Fig. 4d) and is associated with the lattice oxygen (OL) of Bentonite-$ZnWO_4$ and chemisorbed oxygen (OH)[40]. Fig. 4e shows standard carbon peak, it was observed at 285 eV.

The pore structure and surface area of Bentonite-$ZnWO_4$ was studied by nitrogen adsorption–desorption isotherms and the pore size distribution was analysed by Barrett–Joyner–Halenda (BJH) procedure. A steep increase in adsorption volume of N_2 is observed and located in the P/P_0 range of 0.65 to 0.90 (Fig. 5a). This increase is due to the capillary

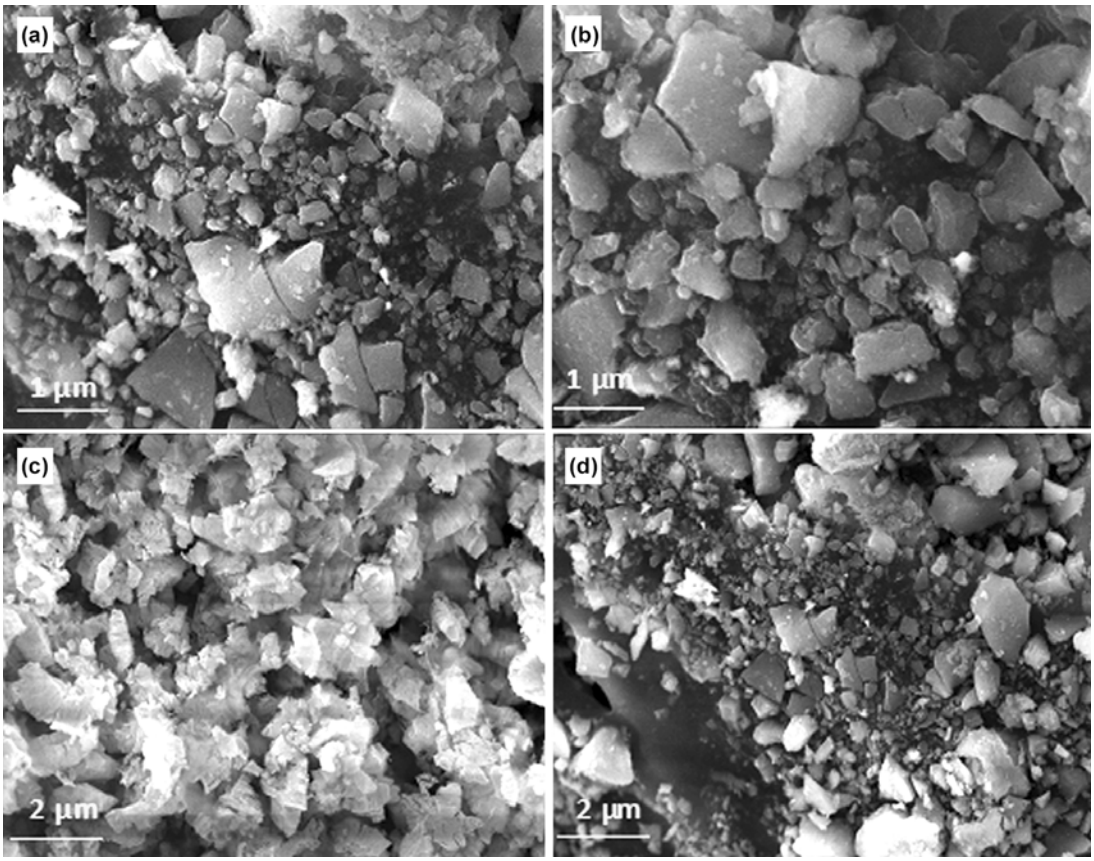

Fig. 2 — FE-SEM images of Bentonite- $ZnWO_4$ at different magnifications: (a,b) 1 µm and (c,d) 2 µm.

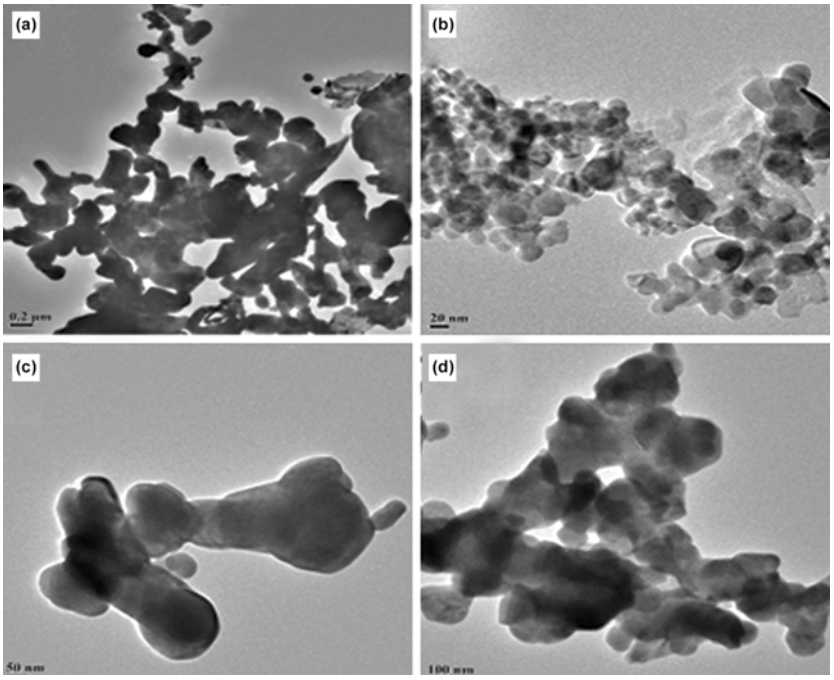

Fig. 3 — FE-TEM images of Bentonite-$ZnWO_4$ at different magnifications (a) 0.2 µm, (b) 20 nm (c) 50 nm, and, (d) 100 nm.

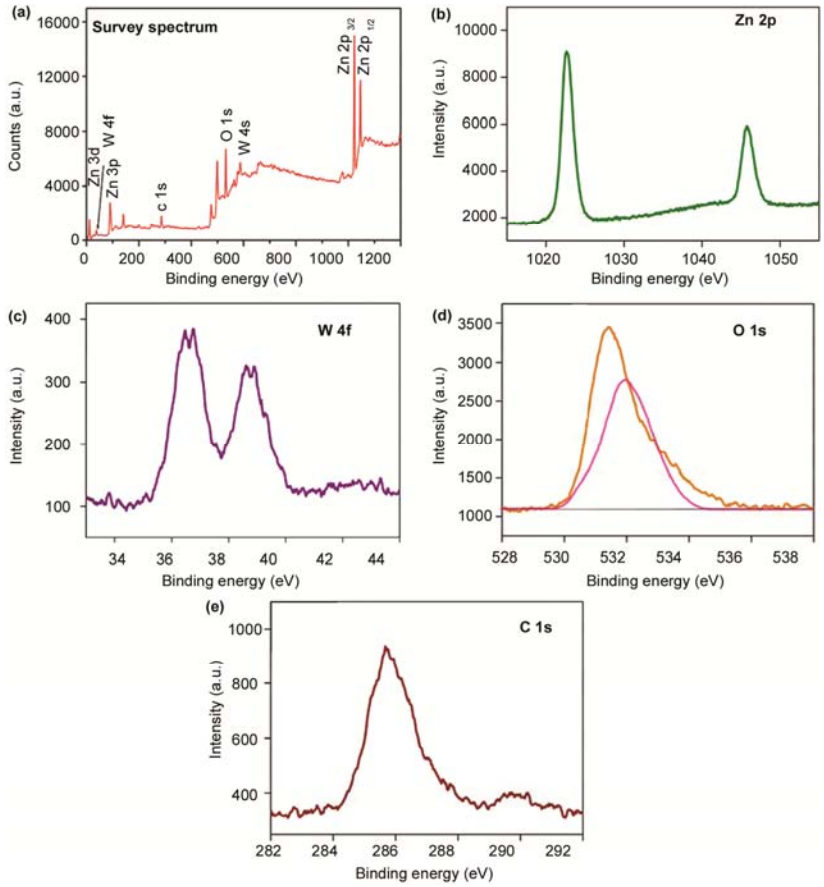

Fig. 4 — XPS Spectra of images of Bentonite-$ZnWO_4$ (a) Survey Spectrum, (b) Zn 2p, (c) W 4f, (d) O 1s, and, (e) C 1s.

condensation, showing the good homogeneity of the catalyst and macroporous size because the P/P_0 position of the inflection point is linked to the pore size. Average pore radius is 188.7 Å which is shown by pore size distribution curve (Fig. 5b). The specific surface area of Bentonite-$ZnWO_4$ is 22.24 m^2g^{-1}, which is more than twice of prepared $ZnWO_4$ (10.72 m^2g^{-1}). Higher BET surface area of Bentonite-$ZnWO_4$ leads to a better photocatalytic activity.

Optical Properties

In order to further explain the photocatalytic mechanism, several factors such as optical absorption, emission property and specific area are interpreted. A material with suitable band gap generates more charge carriers. The diffuse reflectance spectra of prepared $ZnWO_4$ and Bentonite-$ZnWO_4$ are displayed in Fig. 6(a) 1 and 6(a) 2, respectively. Intensity of UV absorption increases two fold when compared to prepare $ZnWO_4$ in the UV region. There is a significant enhancement of visible absorption. This indicates that Bentonite-$ZnWO_4$ can be UV and visible active semiconductor material. It is further confirmed by band gap value of prepared bentonite-$ZnWO_4$ (2.8 eV) (Fig.6 (ii)).

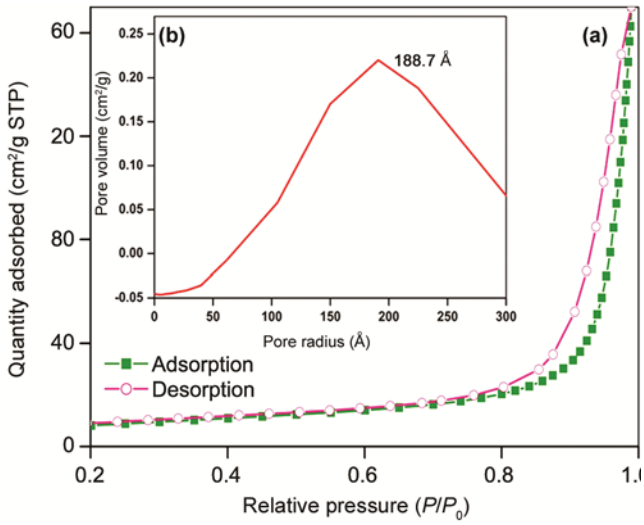

Fig. 5 — BET adsorption–desorption isotherms of (a) Bentonite-$ZnWO_4$, and, (b) their pore size distribution.

Photoluminescence spectra of prepared $ZnWO_4$ and Bentonite-$ZnWO_4$ are shown in Fig. 7a and 7b respectively. The PL intensity of Bentonite-$ZnWO_4$ is less than prepared $ZnWO_4$. The decreased fluorescence intensity means less recombination of electron-hole pairs and better photocatalytic activity.

Photocatalytic measurements

The photocatalytic activity of Rh-B with different photocatalysts under UV irradiation is shown in Fig. 8. About 98% degradation of the dye occurred at the time of 60 min with Bentonite-$ZnWO_4$. But raw Bentonite, prepared ZnO, TiO_2-P25, prepared $ZnWO_4$ gave 30.5, 62.4, 66.2 and 74.2 percentages of degradation under same reaction conditions respectively. This shows that prepared photocatalyst Bentonite-$ZnWO_4$ is more efficient in degradation of Rh-B under UV light than other catalysts. In case of MB dye, 29.5, 67.6, 73.2 and 79.2% of degradations occurred for raw bentonite, prepared ZnO, TiO_2-P25 and prepared $ZnWO_4$ respectively at 60 min irradiation time (Fig. 9).

The removal of Rh-B and MB using Bentonite-$ZnWO_4$ at different irradiation times is shown in Fig. 10. Rh-B and MB undergo 98 and 96 percentage of degradation respectively in 60 min. The UV spectral changes of Rh-B at different irradiation times with Bentonite-$ZnWO_4$ Supplementary Data (Fig. S1) shows regular decrease in intensity without the

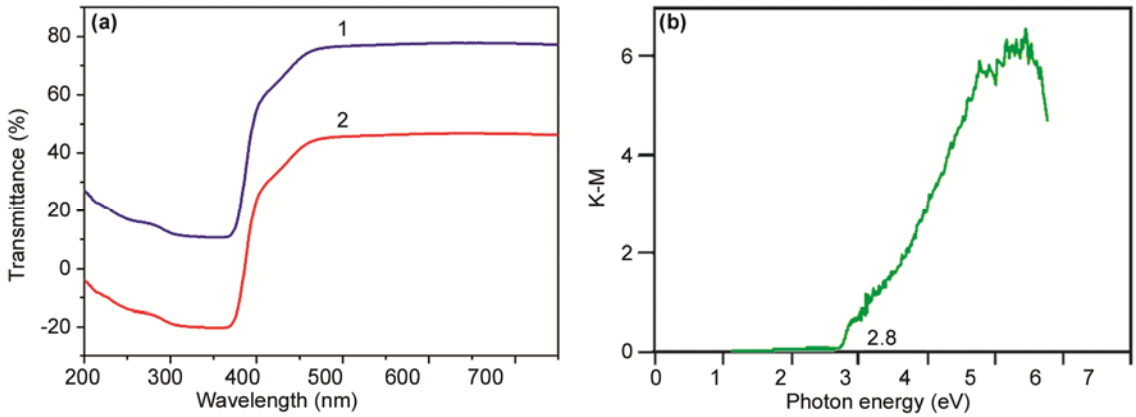

Fig. 6 — (a) Diffuse reflectance spectra of (1) Prepared $ZnWO_4$, and, (2) Bentonite-$ZnWO_4$. (b) Band gap image of Bentonite supported $ZnWO_4$.

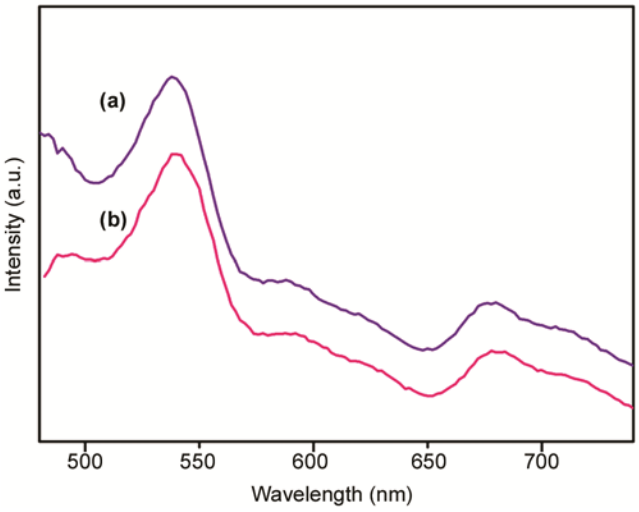

Fig. 7 — Photoluminescence spectra of (a) Prepared $ZnWO_4$, and, (b) Bentonite-$ZnWO_4$.

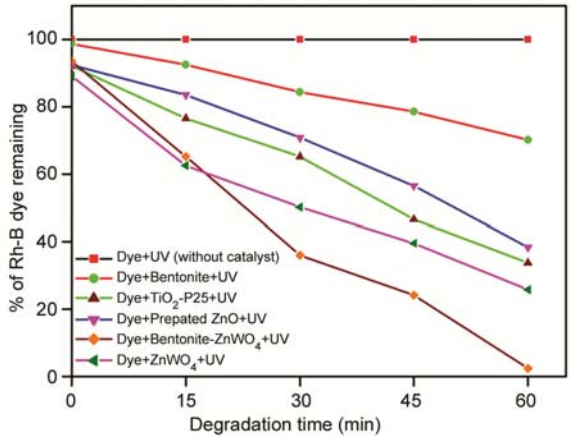

Fig. 8 — Photodegradability of Rh–B with different catalysts: dye concentration = 3×10^{-4} M, catalyst suspended = 3 g L^{-1}, pH = 7, airflow rate = 8.1 mL s^{-1}, I_{UV} = 1.381×10^{-6} einstein L^{-1} s^{-1}. Irradiation time = 60 min.

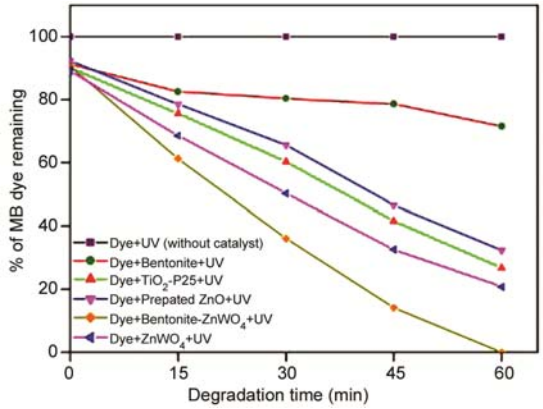

Fig. 9 — Photodegradability of MB with different catalysts: dye concentration = 1×10^{-4} M, catalyst suspended = 3 g L^{-1}, pH = 7, airflow rate = 8.1 mL s^{-1}, I_{UV} = 1.381×10^{-6} einstein L^{-1} s^{-1}. Irradiation time = 60 min.

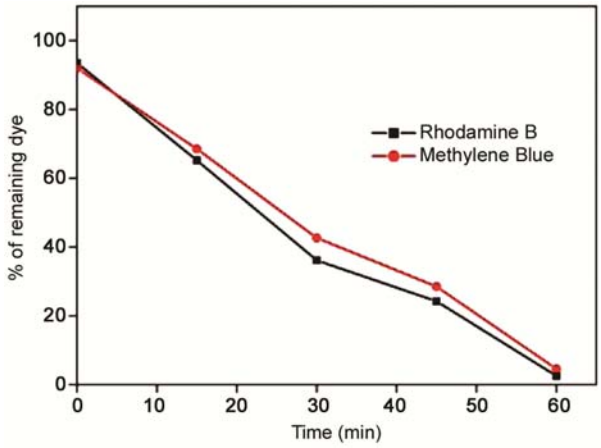

Fig. 10 — Photodegradability comparison of Rh–B and Methylene Blue with different time intervel: dye concentration = 3×10^{-4} M, MB-catalyst =1×10^{-4} M suspended = 3 g L^{-1}, pH = 7, airflow rate = 8.1 mL s^{-1}, I_{UV} = 1.381×10^{-6} einstein L^{-1} s^{-1}.

formation of new absorption peak, which indicates the absence of intermediates absorbing at the analytical wavelength.

Mechanism

Two main reasons for higher degradation efficiency are:

(i) Reflectance of Bentonite Supported $ZnWO_4$ is less than prepared $ZnWO_4$, which shows that Bentonite-$ZnWO_4$ has higher absorbance than $ZnWO_4$. Its band gap energy is reduced to 2.8 eV.

(ii) Higher surface area of Bentonite-$ZnWO_4$ (22.24 m^2g^{-1}) than prepared $ZnWO_4$ (10.72 m^2g^{-1}).

As other semiconductor oxides like ZnO, $ZnWO_4$ on irradiation generates electron and hole, which produce hydroxyl radicals and super oxide radicals. These oxidising species completely mineralise the dye in to mineral salts, CO_2 and H_2O as shown in Scheme 1. Reduction of photoluminescence intensity of Bentonite-$ZnWO_4$, when compared to prepared $ZnWO_4$ indicates the suppression of recombination of the photogenerated electron hole pair by loaded Bentonite on $ZnWO_4$ making the charge separation efficient and show increased photocatalytic activity. In addition to this electron transfer, loaded bentonite has a number of metal/non-metal oxides. Metal ions can generate intermittent energy levels for the reduction of band gap energy and its constituent oxides can reduce the electron-hole recombination[41].

Influence of pH and Reusability

The influence of pH on the photodegradation of Rh-B and MB was analysed in the pH range 3−11,

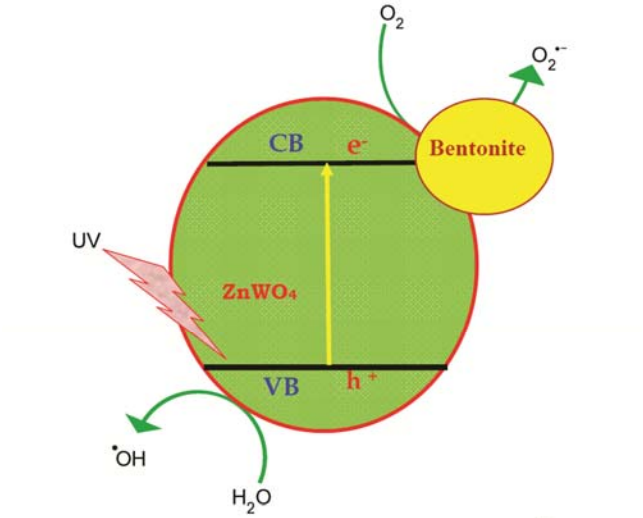

Scheme 1

and the results are given in Supplementary Data, Fig. S2. After 60 min of irradiation, the percentages of Rh-B degradation are 35, 68, 98, 54, and 48% at pH 3, 5, 7, 9, and 11, respectively. MB undergoes 28, 56, 97, 65 and 42% of degradation at pH 3, 5, 7, 9 and 11 respectively. At acidic pH range the removal efficiency is less and it is due to the dissolution of $ZnWO_4$. $ZnWO_4$ can react with acids to produce the corresponding salt at low acidic pH values[42]. At high pH value Bentonite-$ZnWO_4$ surface is negatively charged by means of adsorbed OH^- ions, which may decreases the adsorption of anionic dye molecules. Furthermore, degradation efficiency of a catalyst depends on the adsorption of dye molecules. For both the dye molecules maximum adsorption occurred at pH 7. The adsorption is high at pH 7 and hence, the degradation is most efficient at this pH.

The stability is very important for recycling of heterogeneous catalyst for photoreaction. The recovered catalyst, after degradation, was dried in a hot air oven at 100 °C for 90 min and used for next cycle. The reusability of Bentonite-$ZnWO_4$ was tested by five successive cycles for the degradation of Rh-B and MB under UV-A light and the results are shown in Supplementary Data, Fig. S3. The degradation decreases slightly up to 4th run and no change was observed after 4th cycle. The 4th run gave 92.5 and 93.2% degradation at 60 min irradiation for Rh-B and MB respectively. These results indicate the good stability and reusability of BZW.

Conclusions

A simple hydrothermal-thermal decomposition method was used to prepare natural clay Bentonite supported $ZnWO_4$ nanomaterial without the use of organic solvents and surfactants. FE-SEM images shows that as-synthesized photocatalyst Bentonite-$ZnWO_4$ composed of microflakes and nanoclusters. FE-TEM images shows the uniform distribution of elements indicating the close attachment within oxides and the particles appear as spherical and hexagonal shapes. The photodegradation results showed that 12% Bentonite supported $ZnWO_4$ had the higher efficiency than that of the raw bentonite, prepared $ZnWO_4$ and prepared ZnO for the degradation of basic dyes (Rh-B and MB) at neutral pH 7. The decreased fluorescence intensity of Bentonite-$ZnWO_4$ reveals reduced recombination of electron-hole pairs and better photocatalytic activity. The work in this paper provides a new application for the surface active natural clay bentonite supported coupled metal oxide ($ZnWO_4$) material on the photocatalytic applications at neutral pH 7.

Supplementary Data

Supplementary data associated with this article are available in the electronic form at http://www.niscair.res.in/jinfo/ijca/IJCA_58A(06)637-644_SupplData.pdf.

References

1 Hoffmann M, Martin S & Choi W, *Chem Rev,* 95 (1995) 69.
2 Fujishima A, Zhang X & Tryk D A, *Surf Sci Rep,* 63 (2008) 515.
3 Chen X, Shen S, Guo L & Mao S, *Chem Rev*, 110 (2010) 6503.
4 Kim J & Choi W, *Ene Env S,* 3 (2010) 1042.
5 Wang R, Xin J H, Yang Y, Liu H, Xu L & Hu J, *Appl Surf Sci*, 227 (2004) 312.
6 Wang J, Wang Z, Huang B, Ma Y, Liu Y, Qin X, Zhang X & Dai Y, *Appl Mater Interf*, 4 (2012) 4024.
7 Subash B, Krishnakumar B, Swaminathan M & Shanthi M, *J Mol Catal A: Chem*, 366 (2013) 54.
8 Thirumalai K, Shanthi M & Swaminathan M, *J Nanosci Nanotech*, 17 (2017) 1.
9 Krishnakumar B, Velmurugan R, Subash B & Swaminathan M, *Ind J Chem*, 51A (2012) 580.
10 Selvam K & Swaminathan M, *Tetrahedron Lett*, 51 (2010) 4911.
11 Chen D, G Z. Shen, K. B Tang, H G Zheng & Y T Qian, *Mater Res Bull*, 38 (2003) 1783.
12 Tomaszewicz E, M Kaczmarek S & Fuks H, *J of Rare Earths*, 27 (2009) 569.
13 Chen S J, Zhou J H, Chen X T, Li J, Li L H, Hong J M, Xue Z & You X Z, *Chem Phys Lett*, 375 (2003) 185.
14 Ede S R, Ramadoss A, Nithiyanantham V, Anantharaj S & Kundu S, *Inorg Chem*, 54 (2015) 3851.

15 Gao Y, Huang Y, Li Y, Zhang Q, Cao J, Ho W & Lee S C, *ACS Sust Chem Eng*, 4 (2016) 6912.
16 Zhao X & Zhu Y F, *Environ Sci Technol*, 40 (2006) 3367.
17 Chen S H, Sun S X, Sun H G, Fan W L, Zhao X & Sun X, *J Phys Chem C*, 114 (2010) 7680.
18 Huang Y, Gao Y, Zhang Q, Cao J J, Huang R J, Ho W & Lee S C, *Appl Catal A*, 515 (2016) 170.
19 Itoh M, Katagiri T, Aoki T & Fujita M, *Radiat Meas*, 42 (2007) 545–548.
20 Muthamizh S, Giribabu K, Suresh R, Manigandan R, Munusamy S, Kumar S P, Stephen A & Narayanan V, *AIP Conf Proc*, 6 (2014) 3392.
21 Cavalcante L S, Almeida M A P, Avansi W, Jr Tranquilin R L, Longo E, Batista N C, Mastelaro V R & Li M S, *Cluster Inorg Chem*, 51 (2012) 10675.
22 Qu W M, Wlodrski W & Meyer J U, *Sens Actu B*, 64 (2000) 76.
23 Dai Q L, Song H W, Bai X, Pan G, Lu S, Wang T, Ren X, Zhao H, *J Phys Chem C*, 111(2007) 7586.
24 Wu J, Duan F, Zheng Y & Xie Y, *J Phys Chem C*, 111 (2007) 12866.
25 Schofield P F, Knight K S & Cressey G, *J Mater Sci*, 31 (1996) 2873.
26 Zhang X Y, Wang J D, Liu J K, Yang X H & Lu Y, *Cryst Eng Comm*, 17 (2015) 1129.
27 Yu C L & Yu J C, *Mater Sci Eng B*, 164 (2009) 16.
28 Lin J, Lin J, & Zhu Y F., *Inorg Chem* 46 (2007) 8372.
29 Shi R, Wang Y J, Li D, Xu J & Zhu Y F, *Appl Catal B*, 100 (2010) 173.
30 Vimonses V, Jin B, Chow C W K & Saint C, *Appl Clay Sci*, 43 (2009) 465.
31 Zhou C H & Keeling J, *Appl Clay Sci,* 74 (2013) 3.
32 Toor M, Jin B, Dai S & Vimonses V, *J Ind Eng Chem*, 21 (2015) 653.
33 Nava Y F, Ulmanu M, Anger I, Maranon E & Castrillon L, *Water Air Soil Pollut*, 215 (2010) 239.
34 Vimonses V, Lei S, Jin B & Chow C W K, *Chem Eng J*, 148 (2009) 364.
35 Thirumalai K, Balachandran S, Selvam K & Swaminathan M, *Em Mater Res*, 5 (2016) 264.
36 Yan J, Shen Y, Li F & Li T, *The Sci World J*, (2013) (Article ID 458106) 8.
37 Stankovic N, Logar M, Lukovic J, Pantic J, Miljevic M, Babic B & Mihajlovic A R, *Proc Appl Ceramics*, 5 (2) (2011) 97.
38 Ansari S A, Khan M M, Ansari M O, Lee J & Cho M H, *J Phys Chem C*, 117 (2013) 27023.
39 Biloen P & Pott G T, *J Catal*, 30 (1973) 169.
40 Thirumalai K, Shanthi M & Swaminathan M, *RSC Adv*, 7 (2017) 7509.
41 Thirumalai K, Balachandran S & Swaminathan M, *Mater Chem Phys*, 183 (2016) 191.
42 Li D, Shi R, Pan C, Zhu Y & Zhao H, *Cryst Eng comm*, 13 (2011) 4695.